Glycolytic Disruption Triggers Interorgan Signaling to Nonautonomously Restrict *Drosophila* Larval Growth

Madhulika Rai[1], Hongde Li[1], Robert A. Policastro[1], Gabriel E. Zentner[1], Travis Nemkov[2], Angelo D'Alessandro[2], and Jason M. Tennessen*

[1]Department of Biology, Indiana University, Bloomington, IN 47405, USA

[2]Department of Biochemistry and Molecular Genetics, University of Colorado Anschutz Medical Campus, Colorado, USA

*Corresponding author

Email: jtenness@iu.edu

Key words: *Drosophila melanogaster,* metabolism, glycolysis, interorgan communication, ecdysone

ABSTRACT

Drosophila larval growth requires efficient conversion of dietary nutrients into biomass. Lactate Dehydrogenase (Ldh) and Glycerol-3-phosphate dehydrogenase (Gpdh1) support larval biosynthetic metabolism by maintaining NAD^+/NADH redox balance and promoting glycolytic flux. Consistent with the cooperative functions of Ldh and Gpdh1, the loss of both enzymes, but neither single enzyme, induces a developmental arrest. However, Ldh and Gpdh1 exhibit complex and often mutually exclusive expression patterns, suggesting that the *Gpdh1; Ldh* double mutant lethal phenotype could be mediated nonautonomously. Here we find that the developmental arrest displayed by the double mutants extends beyond simple metabolic disruption and instead stems, in part, from changes in systemic growth factor signaling. Specifically, we demonstrate that this synthetic lethality is linked to the upregulation of Upd3, a cytokine involved in the Jak/Stat signaling pathway. Moreover, we demonstrate that either loss of the Upd3 or dietary administration of the steroid hormone 20-hydroxyecdysone (20E) rescue the synthetic lethal phenotype of *Gpdh1; Ldh* double mutants. Together, these findings demonstrate that metabolic disruptions within a single tissue can nonautonomously modulate interorgan signaling to ensure synchronous developmental growth.

SUMMARY STATEMENT

We used the fruit fly *Drosophila melanogaster* to demonstrate that disruption of glycolysis within a single larval tissue alters systemic cytokine signaling and nonautonomously inhibits development of the entire animal.

INTRODUCTION

Animal development requires the precise integration of environmental and metabolic cues with intrinsic growth signaling pathways (Miyazawa and Aulehla, 2018). Under ideal growth conditions, the metabolic pathways involved in central carbon metabolism efficiently convert dietary nutrients into the necessary biomass and energy to support rapid growth. Conversely, environmental stressors such as starvation, infection, and toxicant exposure necessitate metabolic reprogramming to maintain survival until conditions improve for growth (Bland, 2023, Deng and Kerppola, 2013, Koyama et al., 2020). The coordination between growth and metabolism under stressful environmental conditions, however, is complex as there is a need to monitor and coordinate metabolic flux across all tissues of the developing animal (Kim et al., 2021). When a single tissue encounters metabolic limitations, peripheral tissues must adjust their growth rates to prevent asynchronous development. This topic of interorgan metabolic communication has become a burgeoning area of research, with numerous studies examining how nutrient-sensing proteins and secreted signaling molecules coordinate growth across multiple tissues (Rajan and Perrimon, 2011, Droujinine and Perrimon, 2016, Castillo-Armengol et al., 2019). Nevertheless, the specific metabolic signals that trigger interorgan growth signaling are only beginning to emerge (Baker and Rutter, 2023, Wang and Lei, 2018, Figlia et al., 2020).

The fruit fly *Drosophila melanogaster* is a powerful system for exploring how metabolism is coordinated with developmental growth (Gillette et al., 2021). The ~200-fold increase in body mass that occurs during the four days of *Drosophila* larval development represents an appealing model for exploring metabolic mechanisms that

85 convert nutrients into biomass and energy. In this regard, previous studies revealed that
86 this impressive growth rate is supported by a coordinated increase in the expression of
87 genes involved in glycolysis, the pentose phosphate pathway, as well as *Ldh*
88 (Rechsteiner, 1970, Tennessen et al., 2011, Tennessen et al., 2014). The resulting larval
89 metabolic program exhibits hallmark features of aerobic glycolysis – a specialized form
90 of carbohydrate metabolism that is ideally suited for rapid biomass production.
91 Considering that several types of cancer cells also rely on aerobic glycolysis for growth
92 and survival (Vander Heiden et al., 2009), *Drosophila* larvae present a compelling model
93 to study this biosynthetic state.

94 We previously demonstrated that the larval metabolic program requires the
95 enzymes Ldh and Gpdh1, which cooperatively regulate NAD^+/NADH redox balance and
96 promote glycolytic flux (Li et al., 2019). Intriguingly, while the loss of either single enzyme
97 has minimal effect on overall larval growth, *Gpdh1; Ldh* double mutants experience a
98 developmental arrest, suggesting a functional redundancy, where each enzyme partially
99 compensates for the loss of the other (Li et al., 2019). However, neither Ldh nor Gpdh1
100 are ubiquitously expressed in larvae (Rechsteiner, 1970, Li et al., 2019, Rai et al., 2024),
101 raising questions as to how these enzymes serve compensatory roles if not expressed in
102 a strictly overlapping pattern. Here we address this question by examining the tissue-
103 specific functions of both enzymes.

104 Our analysis of Gpdh1 and Ldh expression during larval development confirms
105 previous observations that these enzymes are expressed in a complex and often mutually
106 exclusive expression pattern (Rechsteiner, 1970). Moreover, we demonstrate that the
107 loss of both enzymes within a single tissue inhibits larval growth in a nonautonomous

manner. Subsequent RNA-seq analysis of *Gpdh1; Ldh* double mutants reveals altered expression of several secreted signaling molecules, including increased expression of the cytokine Upd3, which was previously shown to regulate systemic larval growth in response to cellular stress (Romao et al., 2021). Using a genetic approach, we find that *upd3; Gpdh1; Ldh* triple mutants can survive larval development and eventually eclose into adults, indicating that increased Upd3 expression serves a significant role in the synthetic lethal phenotype of *Gpdh1; Ldh* double mutants. Finally, we demonstrate that the steroid hormone 20E also plays a role in this phenotype, as a dietary supplement of 20E also allows *Gpdh1; Ldh* double mutants to complete larval development. Overall, our findings reveal that the developmental delay and lethal phenotype associated with *Gpdh1; Ldh* double mutants are not simply the result of metabolic failure but rather stem, in part, from changes in systemic growth signaling.

121 **RESULTS AND DISCUSSIONS**

122 **Ldh and Gpdh1 influence larval tissue growth in a nonautonomous manner**

123 To better understand how Ldh and Gpdh1 cooperatively promote *Drosophila*
124 larval growth, we examined the spatial expression pattern of both enzymes. Our
125 analysis revealed that Ldh and Gpdh1 are often expressed in a mutually exclusive
126 manner. In the Malpighian tubules, for example, *Ldh* is expressed in the stellate cells
127 while *Gpdh1* is primarily expressed in principal cells (Figure 1A-A'''). Similarly, cells of
128 the larval midgut tend to express high levels of either Ldh or Gpdh1, but rarely do we
129 observe a cell expressing both enzymes (Figure 1B-B''', S1A-D). This trend is also
130 apparent in the central nervous system, where although both *Ldh* and *Gpdh1* are co-
131 expressed in many cells the CNS, *Gpdh1*, but not *Ldh*, is expressed in neural stem
132 cells and the prothoracic gland (Figure 1C-D''' and S1E-H). Finally, both the fat body
133 and salivary glands express Gpdh1 but not Ldh (Figure 1A-A''', S1I-P), a result that is
134 consistent with previous observations. In fact, the only tissue where we consistently
135 observed uniform and overlapping expression of both enzymes was in the larval body
136 wall muscle (Figure 1E-E''').

137 The complex *Ldh* and *Gpdh1* expression patterns raise the question as to how
138 these enzymes cooperatively regulate larval metabolism if they are not present in the
139 same cells and tissues. One explanation is that loss of one enzyme alters the spatial
140 expression pattern of the other; however, we find no evidence to support this
141 hypothesis. For example, Ldh expression is nearly undetectable in wild-type salivary
142 glands and is not increased in *Gpdh1* mutant salivary glands (Figure S2A-G). Similarly,
143 salivary gland Gpdh1 expression is not further elevated in *Ldh* mutants (Figure S2H-

144 N). We also observe no increase in Ldh expression within the fat body of *Gpdh1*
145 mutants (Figure S3A-G), although we do see a slight increase in Gpdh1 expression
146 within *Ldh* mutant fat bodies (Figure S3 H-N). These results are also consistent with a
147 previous observation that Gpdh1 levels are not increased in *Ldh* mutant clones within
148 the larval CNS (Li et al., 2019).

149 Our findings suggest that the *Gpdh1; Ldh* double mutant growth defects are not
150 simply the combined result of metabolic dysfunction within individual cells, but rather
151 stem from changes in interorgan signaling. We tested this hypothesis by using RNAi
152 to deplete *Ldh* expression in the muscle (*Mef2R-GAL4)* and fat body (*r4-GAL4*) of
153 *Gpdh1* mutant larvae. With both drivers, loss of the two enzymes within a single tissue
154 significantly reduced larval growth (Figure 2A, S4A) and slowed development as
155 determined by time to pupation (Figure 2B, S4B). Moreover, these developmental
156 delays were apparent in tissues not expressing the *Ldh-RNAi* transgene – for example,
157 the salivary glands of age-matched *Gpdh1; Mef2R-Ldh-RNAi* larvae were significantly
158 smaller than those of either the wild-type control, *Gpdh1* mutant, or *Mef2R-Ldh-RNAi*
159 animals (Figure 2C-F). Together, these results suggest that loss of both enzymes
160 within a single tissue can globally influence larval growth and development.

161

162 **Upd3 is required to arrest larval growth in *Gpdh1; Ldh* double mutants**

163 To better understand how Ldh and Gpdh1 nonautonomously regulate larval
164 development, we used RNA-seq to analyze gene expression in $Ldh^{16/17}$ mutants,
165 $Gpdh1^{A10/B18}$ mutants, and $Gpdh1^{A10/B18}$; $Ldh^{16/17}$ double mutants relative to
166 genetically-matched heterozygous controls (Table S1). While our approach identified

167 several genes that were significantly changed in both single mutants (Figure 3A-B
168 and S5), for the purpose of this analysis we focused on those genes that were only
169 altered in double mutants (Table S2). Among the genes that were significantly down-
170 or up-regulated in *Gpdh1*$^{A10/B18}$*; Ldh*$^{16/17}$ double mutants but not the single mutants, we
171 identified four secreted factors that were previously shown to systemically regulate
172 larval growth and metabolism: *peptidoglycan recognition protein SC2* (*PGRP-SC2*;
173 FBgn0043575), *peptidoglycan recognition protein LA*, (*PGRP-LA*; FBgn0035975),
174 *dawdle* (*daw*; FBgn0031461), and *unpaired 3* (*upd3*; FBgn0053542) (Droujinine and
175 Perrimon, 2016, Musselman et al., 2018, Romao et al., 2021). While each of these
176 molecules is known to function in interorgan communication and could contribute
177 towards regulating the growth of *Gpdh1; Ldh* double mutants, we decided to focus on
178 the cytokine Upd3 for the remainder of this study.

179 Our RNA-seq analysis indicates that *upd3* expression is significantly elevated
180 in *Gpdh1; Ldh* double mutants. Considering that Upd3 inhibits larval development in
181 response to both environmental and intracellular stress (Droujinine and Perrimon,
182 2016, Romao et al., 2021, Yang et al., 2015), increased expression of this cytokine
183 could serve a role in the *Gpdh1; Ldh* developmental arrest phenotype. We tested this
184 possibility by generating *upd3*$^{\Delta}$*; Gpdh1*$^{A10/B18}$*; Ldh*$^{16/17}$ triple mutants, with the
185 hypothesis that loss of Upd3 signaling in the double mutant background would
186 suppress the larval arrest phenotype. Indeed, triple mutants completed larval
187 development and entered metamorphosis at a significantly higher rate than the double
188 mutants (Figure 3C-D). Moreover, while we never observed a *Gpdh1*$^{A10/B18}$*; Ldh*$^{16/17}$
189 double mutant complete metamorphosis, up to 30% of triple mutant larvae survived to

190 adulthood (Figure 3E-F). We would note, however, that *upd3*$^{\Delta}$*; Gpdh1*$^{A10/B18}$*; Ldh*$^{16/17}$
191 triple mutants were significantly smaller than controls, sick, and died within 2-3 days of
192 eclosion, indicating that not all aspects of the *Gpdh1*$^{A10/B18}$*; Ldh*$^{16/17}$ double mutant
193 phenotype are regulated by Upd3.

194 To better understand how the *upd3* mutations suppress the *Gpdh1*$^{A10/B18}$*;*
195 *Ldh*$^{16/17}$ larval arrest phenotype, we examined both double and triple mutant larvae
196 using a semi-targeted metabolomics approach (Table S3). Our analysis revealed no
197 significant metabolic differences between the two strains (Figure S6). Notably, the
198 levels of both lactate and glycerol-3-phosphate were unchanged in the triple mutant as
199 compared with double mutant larvae (Figure S6B-C), indicating that the *upd3* mutation
200 does not restore glycolytic metabolism in *Gpdh1*$^{A10/B18}$*; Ldh*$^{16/17}$ double mutants.
201 Overall, these results suggest that *Gpdh1*$^{A10/B18}$*; Ldh*$^{16/17}$ double mutants do not simply
202 die from metabolic dysfunction but rather experience a larval arrest due, in part, to
203 increased Upd3 signaling.

204

205 **Ecdysone feeding is sufficient to suppress the *Gpdh1; Ldh* larval lethal phenotype.**

206 To further explore the connection between Upd3 and the *Gpdh1*$^{A10/B18}$*; Ldh*$^{16/17}$
207 larval arrest phenotype, we used a *10XStat92E-GFP* reporter to identify those tissues
208 with increased JAK/STAT signaling (Yang et al., 2015, Ekas et al., 2006). Consistent with
209 Upd3 serving a key role in limiting systemic growth, *Gpdh1*$^{A10/B18}$*; Ldh*$^{16/17}$ double mutants
210 exhibited widespread *10XStat92E-GFP* reporter expression when compared with either
211 the heterozygous control strain, *Ldh*$^{16/17}$ single mutant, or *Gpdh1*$^{A10/B18}$ single mutant. In
212 this regard, we observed increased *10XStat92E-GFP* expression in the fat body (Figure

213 S7A-D), salivary glands (Figure S7E-H), muscles (Figure S7I-L), and CNS (Figure 4A-D).
214 Intriguingly, we also observed significantly increased *10XStat92E-GFP* expression in the
215 prothoracic gland (PG) of double mutants relative to the single mutants (Figure 4A-D),
216 although, we would note that *Gpdh1*$^{A10/B18}$ single mutants displayed elevated
217 *10XStat92E-GFP* expression relative to either the *Ldh*$^{16/17}$ single mutant or heterozygous
218 control strain (Figure 4B).

219 A previous study of tumorous wing discs demonstrated that Upd3 signaling can
220 suppress ecdysone production in the PG and inhibit larval development (Romao et al.,
221 2021). Thus, our observation that *10XStat92E-GFP* expression is elevated within the
222 *Gpdh1*$^{A10/B18}$*; Ldh*$^{16/17}$ PG raises the possibility that the double mutant larval arrest
223 phenotype stems, in part, from decreased ecdysone signaling. Consistent with this model,
224 we found that the addition of 20-hydroxyecdysone (20E; the active form of ecdysone) to
225 the larval food significantly increased the pupariation rate of *Gpdh1*$^{A10/B18}$*; Ldh*$^{16/17}$ double
226 mutants (Figure 4E). Overall, these results indicate that changes in 20E signaling
227 contribute to the *Gpdh1*$^{A10/B18}$*; Ldh*$^{16/17}$ double mutant synthetic lethal phenotype.

228

229 **Redefining the developmental functions of "Housekeeping Genes"**

230 Our studies unexpectedly reveal that *Drosophila* larval development can tolerate
231 loss of two key enzymes that regulate cytosolic NAD^+/NADH balance. These findings,
232 while surprising, are consistent with classic studies of *COX5A* (also known as *tenured*),
233 which revealed that loss of this electron transport chain subunit induces a specific eye
234 development phenotype (Mandal et al., 2005). The defects induced by *COX5A* mutations
235 are not simply the result of defects in ATP synthesis, but rather stem from the activation

236 of a pathway involving AMPK and p53, which eliminates Cyclin E and induces a cell cycle
237 arrest (Mandal et al., 2005). These foundational observations were subsequently
238 validated by both follow-up studies and a large-scale genetic screen, which demonstrated
239 that depletion of many genes that encode electron transport chain subunits induce distinct
240 defects in eye development (Liao et al., 2006, Pletcher et al., 2019). Our findings are built
241 upon these earlier studies and again demonstrate that *Drosophila* larvae experiencing
242 severe metabolic disruptions don't simply die due to metabolic stress, but instead arrest
243 development through the activity of specific growth signaling pathways. Specifically, our
244 findings suggest that loss of both Gpdh1 and Ldh activate a previously described
245 feedforward loop, in which elevated Upd3 signaling repressed 20E signaling (Romao et
246 al., 2021).

247 Conceptually, our findings offer an interesting mechanistic rationale explaining
248 how animals in the wild might cope with developmental delays as a function of exposure
249 to severe metabolic stressors. While factors such as starvation and hypoxia inevitably
250 induce cell autonomous responses involving the entire organism (Schito and Rey, 2018),
251 animals also encounter environmental insults that affect individual tissues, including
252 bacterial and parasitic infections, toxins that target specific organs, and nutrient
253 imbalances that impinge upon cell-specific metabolic bottlenecks (Koyama et al., 2020).
254 Animal development has evolved to identify these tissue-specific metabolic stresses and
255 produce signals from effected cells that are subsequently amplified and recognized by
256 unaffected tissues, thus allowing development to be delayed in a coordinate manner. For
257 example, *Drosophila* hemocytes respond to parasitic wasp infections by inducing a cell
258 intrinsic increase in glycolytic metabolism that not only facilitates an effective immune

259 response but also produces an adenosine signal that remodels peripheral metabolism
260 (Bajgar et al. 2015, Bajgar and Dolezal, 2018).

261 Our findings that Upd3 and 20E are part of a coordinated response to tissue-
262 specific disruption of glycolytic flux provide new insights into the coordination between
263 metabolism and developmental growth. Upd3 has emerged as a common stress-induced
264 cytokine that communicates cell-specific information with peripheral tissues (Woodcock
265 et al., 2015, Gera et al., 2022), and our finding reinforces a previously proposed model
266 in which elevated Upd3 signaling induces a feedforward loop that inhibits 20E signaling
267 and delays *Drosophila* development (Romao et al., 2021). In this regard, the involvement
268 of a steroid hormone is an important feature of the regulatory mechanism, as it allows for
269 a single tissue to indirectly influence the developmental progression of entire animal.
270 Moving forward, the key question emerges of how metabolic stress regulates Upd3
271 signaling? Both individual metabolites as well end products of cell-specific metabolic
272 dysfunction (e.g., redox imbalance and ROS accumulation) represent potential signals
273 that could trigger Upd3 signaling as well as related modes of interorgan communication.
274 Regardless of the answer, our study highlights that core metabolic enzymes are not
275 simple products of “housekeeping genes,” but rather serve dynamic cellular functions that
276 are fully integrated into the signaling pathways that regulate multicellular growth and
277 development.

278

METHODS

Drosophila melanogaster husbandry and genetic analysis

Fly stocks were maintained at 25ºC on Bloomington Drosophila Stock Center (BDSC) food. Larvae were raised and collected as previously described (Li and Tennessen, 2017). Unless noted, *Ldh* mutant larvae harbored a trans-heterozygous combination of Ldh^{16} (RRID:BDSC_94698) and Ldh^{17} (RRID:BDSC_94699) (Li and Tennessen, 2017) and *Gpdh1* mutant larvae harbored a trans-heterozygous combination of $Gpdh1^{A10}$ (RRID:BDSC_94702) and $Gpdh1^{B18}$ (RRID:BDSC_94703) (Li et al., 2019). The *upd3* mutant strain was obtained from the BDSC (RRID:BDSC_55728). The $Ldh\text{-}GFP^{Genomic}$ stock (RRID:BDSC_94704) used for colocalization analysis of Ldh and Gpdh1 was previously described (Bawa et al., 2020; Rai et al., 2024). The *w[1118]; P{w[+mC]=10XStat92E-GFP}2* stock was obtained from the BDSC (RRID:BDSC_26198) and recombined with Ldh^{16} to visualize STAT expression levels in the tissues of ($Gpdh1^{A10/B18}$) double mutant larvae. Tissue specific knockdown of Ldh was conducted using transgenes that express GAL4 in either muscle (P{w[+mC]=GAL4-Mef2.R}3; RRID:BDSC_27390) or fat body (P{w[+mC]=r4-GAL4}3; RRID:BDSC_33832). RNAi experiments were conducted using transgenes that targeted *Ldh* expression (RRID:BDSC_33640). Each of these Gal4 lines were placed into a $Gpdh1^{B18}$ mutant background and crossed to w^{1118}; $Gpdh1^{A10}$; *UAS-Ldh-RNAi* to attain the tissue specific knockdown. Flybase was used as an essential reference tool throughout this study (Gramates et al., 2022, Ozturk-Colak et al., 2024).

Immunofluorescence

302 Larval tissues were dissected in 1X phosphate buffer saline (PBS; pH7.0) and fixed
303 with 4% paraformaldehyde in PBS for 30 minutes at room temperature. Fixed samples
304 were subsequently washed once with PBS and twice with 0.3% PBT (1x PBS with
305 Triton X-100) for 10 mins per wash.

306 For GFP antibody staining, fixed tissues were incubated with goat serum
307 blocking buffer (4% Goat Serum, 0.3% PBT) for one hour at RT and stained overnight
308 at 4 ºC with primary antibody Rabbit anti-GFP diluted 1:500 (#A11122 Thermo
309 Fisher). Samples were washed three times using 0.3% PBT and stained with
310 secondary antibody Alexa Fluor 488 Goat anti-Rabbit diluted 1:1000 (#R37116;
311 Thermo Fisher) for either 4 hrs at room temperature or overnight at 4 ºC. Stained
312 tissues were washed with 0.3% PBT, immersed in DAPI (0.5µg/ml 1X PBS) for 15
313 mins and then mounted with a vector shield with DAPI (Vector Laboratories; H-1200-
314 10).

315 Ldh protein expression was visualized using an anti-Ldh antibody (Boster bio
316 DZ41222) as previously described (Rai et al., 2024). For larval tissues staining with
317 anti-Gpdh1 antibody (Boster Bio DZ41223), the same protocol was used as for anti-
318 Ldh staining, except that the anti-Gpdh1 antibody was diluted 1:100.

319

320 **Mounting and imaging**

321 All the stained tissues were mounted using VECTASHIELD containing DAPI (Vector
322 Laboratories; H-1200-10). Multiple Z-scans of individual tissues were acquired using
323 the Leica SP8 confocal microscope in the Light Microscopy Imaging Center at Indiana
324 University, Bloomington. Unless noted, figure panels contain a representative Z-scan.

325 For presenting the Z stack in a 2D image, the Z projection tool of Fiji was used, with
326 maximum projection.
327 Quantification of Gpdh1 and Ldh antibody staining was conducted by measuring
328 the mean intensities for Gpdh1, Ldh and DAPI in the region of interest (ROI) per image,
329 using Fiji. Gpdh1 and Ldh mean intensities were normalized to the mean DAPI intensity
330 for the same ROI per image and plotted by using GraphPad Prism v10.1. Statistical
331 analysis was conducted using the Mann-Whitney test.
332
333 **Imaging and quantification of larval size**
334 Third instar larvae were collected and imaged using Leica MZ 10F microscope.
335 The size of the larvae was measured by drawing a line from posterior to anterior end
336 and noting down the total length by using Fiji. Data was plotted by using GraphPad
337 Prism v10.1. Statistical analysis was conducted using the Mann-Whitney test.
338
339 **Adult imaging**
340 Third instar wandering larvae were kept on a molasses agar plate with yeast
341 paste. Starting on D9 after egg laying, pupae were checked for eclosion, and the newly
342 eclosed adults were collected into a BDSC food vial. Adults were imaged by using
343 Leica DFC 450.
344
345 **Percentage pupation**
346 The pupation rate was calculated by placing 20 synchronized L1 larvae of each
347 genotype on a molasses agar plate with yeast paste. Starting on day 4 after egg laying,

plates were monitored every 24 hours for pupae.

Sample collection and extraction for Metabolomics Analysis

Mutant and control larvae were collected at the mid-L2 stage (~60 hours after egg-laying at 25ºC) and extracted as previously described (Li and Tennessen, 2018). Briefly, collected larvae were placed into a prechilled 1.5 mL centrifuge tube on ice, washed with ice-cold water, and immediately frozen in liquid nitrogen. For extraction, larvae were transferred to pretared 1.4 mm bead tubes, the mass was measured using a Mettler Toledo XS105 balance, and the sample was returned to a liquid nitrogen bath prior to being stored at -80°C . Samples were subsequently homogenized in 0.8 mL of prechilled (-20 °C) 90% methanol containing 2 µg/mL succinic-d4 acid, for 30 seconds at 6.45 m/s using a bead mill homogenizer located in a 4°C temperature control room. The homogenized samples were incubated at -20 °C for 1 hour and then centrifuged at 20,000 × g for 5 min at 4°C. The resulting supernatant was sent for metabolomics analysis at the University of Colorado Anschutz Medical Campus, as previously described (Nemkov et al., 2019).

Statistical analysis of metabolite data

The metabolomics dataset was analyzed using Metaboanalyst version 6.0 (Pang et al., 2024) with data normalized to sample mass and preprocessed using log normalization and Pareto scaling. Graphs for the relative levels of individual metabolites were plotted by using GraphPad Prism v10.1. Statistical analysis for these graphs were conducted using a Mann-Whitney test.

372

373 **Transcriptomic analysis**

374 Quality control of reads performed with FastQC v0.11.9
375 (https://www.bioinformatics.babraham.ac.uk/projects/fastqc/). Read quantification to
376 transcripts was accomplished with Salmon v1.4.0 (Patro et al., 2017) using the
377 ENSEMBL D. melanogaster BDGP6.28 cDNA sequences file, and the softmasked
378 toplevel ENSEMBL BDGP6.28 genome assembly as the decoy sequences. Reads
379 were imported into R and aggregated into gene counts using tximport v1.18.0
380 (Soneson et al., 2015), and differential expression was performed using DESeq2
381 v1.30.0 (Love et al., 2014)

382

383 **Ecdysone feeding**

384 Larvae were fed ecdysone in a modified molasses agar food. 115 mL of
385 molasses and 24 grams of agar were added to 750 mL of boiling water on a stirring
386 hot plate. The temperature was then reduced to 60ºC and 5 grams of yeast was added
387 to the media, at which point 2 mL of media was pipetted into a 35 mm petri dish. The
388 low agar concentration resulted in a semi-solid media gained a semi-solid texture that
389 was suitable for diffusion of a 20E stock solution.

390 A 30 mM stock solution of 20E (Sigma H5142) was prepared in 90% ethanol
391 and 3.33 μL of stock solution was added to the modified molasses food, resulting in a
392 final concentration of 50 μM (Ono, 2014; Koyama et al., 2014). Larvae of the tested
393 genotypes were transferred to the 20E-supplemented food plates immediately after
394 hatching and subsequently transferred to fresh 20E-supplemented plates every 24 hrs.

ACKNOWLEDGEMENTS

We thank the Bloomington *Drosophila* Stock Center (NIH P40OD018537) for providing fly stocks, the *Drosophila* Genomics Resource Center (NIH 2P40OD010949) for genomic reagents, Flybase (NIH 5U41HG000739), and the Indiana University Light Microscopy Imaging Center. Thanks to Shefali Shefali for critical comments on the manuscript.

COMPETING INTERESTS

No competing interests declared

FUNDING

J.M.T. is supported by NIH 1R35GM119557.

DATA AVAILABILITY

The RNA-seq data discussed in this publication have been deposited in NCBI's Gene Expression Omnibus (Edgar *et al*., 2002) and are accessible through GEO Series accession number GSE119334 (https://www.ncbi.nlm.nih.gov/geo/query/acc.cgi?acc=GSE119334) and GSE121876 (https://www.ncbi.nlm.nih.gov/geo/query/acc.cgi?acc=GSE121876). Supplemental Tables S1-S3 are available at https://doi.org/10.6084/m9.figshare.25984402.v1.

.

415 **FIGURE LEGENDS**

416 **Figure 1. *Ldh* and *Gpdh1* expression patterns are complex and non-strictly**
417 **overlapping.** Representative confocal images of second instar larval tissues expressing
418 *Ldh-GFP*^{Genomic} and immuno-stained with αGpdh1 antibody. DAPI is shown in blue, Ldh-
419 GFP and Gpdh1 are represented in green and magenta, respectively. The rightmost
420 panel displays the merged images of Ldh-GFP and Gpdh1 staining. (A-A'') Malpighian
421 tubules, (B-B'') gut, (C-C'') ventral side of CNS, (D-D'') magnification of the outlined
422 region of interest in (C-C''), and (E-E'') muscles. Arrows denote non-overlapping Ldh
423 expression. The scale bar represents 40 μM. The scale bar in (A) applies to all panels.

424

425 **Figure 2. Tissue-specific loss of Ldh and Gpdh1 induces systemic growth defects.**
426 Growth and development of both control (*Mef2R-Gal4* and *UAS-Ldh-RNAi* strains) and
427 mutant strains (*Gpdh1*$^{A10/B18}$ mutants, *Mef2R-Ldh-RNAi*, and *Gpdh1*$^{A10/B18}$*; Mef2R-Ldh-*
428 *RNAi*) were monitored throughout larval development. (A) Representative images of L2
429 larvae (60 hr AEL) from the indicated genotypes. The scale bar represents 1 mm. (B-C)
430 Quantification of (B) larval length and (C) time to pupation from the indicated genotypes.
431 All experiments were repeated a minimum of three times. n≥5 biological replicates for (B,
432 C). Error bars represent standard deviation; *P<0.05, ***P<0.0001. P-values were
433 calculated using the Mann-Whitney test. (D-G) Representative images of salivary glands
434 dissected from the indicated genotypes. DAPI is shown in blue. The scale bar represents
435 40 μM. The scale bar in (D) applies to (E).

436

437 **Figure 3. An *upd3* mutation suppresses the synthetic lethal phenotype of *Gpdh1;***
438 ***Ldh* double mutants.** (A-B) Venn diagrams showing the overlap between the number of
439 genes that were either (A) downregulated or (B) upregulated in either single mutant
440 ($Gpdh1^{A10/B18}$ and $Ldh^{16/17}$) as well as the double mutant ($Gpdh1^{A10/B18}$; $Ldh^{16/17}$) relative
441 to the respective heterozygous controls strains. Associated tables in (A, B) list secreted
442 factors that are only dysregulated in the $Gpdh1^{A10/B18}$; $Ldh^{16/17}$ double mutant. (C)
443 Representative larval images of the indicated genotypes. The scale bars represent 1 mm
444 and apply to all panels. (D) Quantification of the larval size for the indicated genotypes.
445 (E) A significant number of male and female triple mutant pupae ($upd3^{\Delta}$; $Ldh^{16/17}$;
446 $Gpdh1^{A10/B18}$) successfully eclosed whereas all $Gpdh1^{A10/B18}$; $Ldh^{16/17}$ died during
447 metamorphosis. The scale bar represents 1mm and applies to all panels. (F) The rate of
448 eclosion was quantified for pupae of the indicated genotypes. Note that no eclosion was
449 observed among vials containing $Gpdh1^{A10/B18}$; $Ldh^{16/17}$ pupae. All experiments are
450 repeated a minimum of three times. n≥5 biological replicates. Error bars represent
451 standard deviation; $^{**}P<0.05$. *P*-values were calculated by using a Mann-Whitney test.
452
453 **Figure 4. Dietary supplementation with 20E suppresses the synthetic lethal**
454 **phenotype of *Gpdh1; Ldh* double mutants.** (A-D) Representative confocal images of
455 *Stat-GFP* expression in the CNS of $Gpdh1^{A10/B18}$; $Ldh^{16/17}$ double mutants as compared
456 to the heterozygous control ($Gpdh1^{A10/+}$; $Ldh^{16/+}$) and single mutant strains ($Gpdh1^{A10/B18}$
457 and $Ldh^{16/17}$). DAPI is shown in blue and *Stat-GFP* expression in green. The scale bar in
458 (A) represents 40 μM and applies to (B-D). (E) A graph illustrating the percent of
459 $Gpdh1^{A10/B18}$; $Ldh^{16/17}$ double mutant that pupariate when raised on yeast-molasses agar

460 that contains either ecdysone or the solvent (ethanol) control. All experiments are
461 repeated a minimum of three times. n=9 biological replicates. Error bars represent
462 standard deviation. ***P*<0.05. *P* value was calculated using a Mann-Whitney test.
463
464
465

466 **SUPPLEMENTARY FIGURE LEGENDS**

467 **Supplementary Figure 1. Ldh and Gpdh1 expression patterns in the CNS, fat body,**
468 **salivary gland, and intestine.** Representative confocal images of second instar larval
469 tissues expressing *Ldh-GFP*^{Genomic} and immuno-stained with αGpdh1 antibody. DAPI is
470 shown in blue, Ldh-GFP and Gpdh1 are represented in green and magenta, respectively.
471 The rightmost panel displays the merged images of Ldh-GFP and Gpdh1 staining. (A-D)
472 Dorsal side of CNS, (E-H) at body (I-L) salivary gland (M-P) gut. The scale bar in all the
473 images represents 40 μM. The scale bar in (A) applies to (B-L) and the scale bar in (M)
474 applies to (N,O,P).

475

476 **Supplementary Figure 2. Characterization of either Ldh or Gpdh1 expression in**
477 **larval tissues following loss of the other enzyme.** Quantification of Ldh and Gpdh1
478 expression in the salivary glands of the heterozygous control strain (*Gpdh1*$^{A10/+}$*; Ldh*$^{16/+}$)
479 and each single mutant strain (*Gpdh1*$^{A10/B18}$ and *Ldh*$^{16/17}$). (A-F) Representative confocal
480 images of (A-C) Ldh expression and (D-F) DAPI staining in all three genotypes. (G) Ldh
481 staining was quantified in the salivary glands of all three genotypes. (H-M) Representative
482 confocal images of (H-J) Gpdh1 expression and (K-M) DAPI staining in all three
483 genotypes. (N) Gpdh1 staining was quantified in the salivary glands of all three
484 genotypes. The scale bar in all images represents 40 μM. The scale bar in (A) applies to
485 (B-F) and the scale bar in (H) applies to (I-M). (G, N) All experiments are repeated a
486 minimum of three times. n=4 biological replicates. Error bars represent standard
487 deviation. $^{**}P < 0.01$. $^{*}P < 0.05$. *P*-values were calculated by using the Mann-Whitney test.

488

489 **Supplementary Figure 3. Characterization of either Ldh or Gpdh1 expression in**
490 **larval fat body following loss of the other enzyme.** Quantification of Ldh and Gpdh1
491 expression in the larval fat body of the heterozygous control strain (*Gpdh1*$^{A10/+}$*; Ldh*$^{16/+}$)
492 and each single mutant strain (*Gpdh1*$^{A10/B18}$ and *Ldh*$^{16/17}$). (A-F) Representative confocal
493 images of (A-C) Ldh expression and (D-F) DAPI staining in all three genotypes. (G) Ldh
494 staining was quantified in the fat body of all three genotypes. (H-M) Representative
495 confocal images of (H-J) Gpdh1 expression and (K-M) DAPI staining in all three
496 genotypes. (N) Gpdh1 staining was quantified in the larval fat body of all three genotypes.
497 The scale bar in all images represents 40 μM. The scale bar in (A) applies to (B-F) and
498 the scale bar in (H) applies to (I-M). (G, N) All experiments are repeated a minimum of
499 three times. N=4 biological replicates. Error bars represent standard deviation. $^{**}P < 0.01$.
500 $^{*}P < 0.05$. *P*-values were calculated by using the Mann-Whitney test.
501
502 **Supplementary Figure 4. Fat body expression of a *Ldh-RNAi* transgene in the fat**
503 **body of *Gpdh1* mutants induces systemic growth defects.** Growth and development
504 of both control (*r4-Gal4* and *UAS-Ldh-RNAi* strains) and mutant strains (*Gpdh1*$^{A10/B18}$
505 mutants, *r4-Ldh-RNAi*, and *Gpdh1*$^{A10/B18}$*; r4-Ldh-RNAi*) were monitored throughout larval
506 development. (A) Representative images of L2 larvae (60 hr AEL) from the indicated
507 genotypes. The scale bar represents 1 mm. (B-C) Quantification of (B) larval length and
508 (C) time to pupation of the indicated genotypes. (B, C) All experiments are repeated a
509 minimum of three times. n≥6 biological replicates. Error bars represent standard
510 deviation. $^{*}P<0.05$ and $^{**}P<0.01$ when compared with all other genotypes. *P*-values were
511 calculated using the Mann-Whitney test.

512

513 **Supplementary Figure 5. RNA-seq analysis of *Ldh* mutants, *Gpdh1* mutants, and**
514 ***Gpdh1, Ldh* double mutants.** Volcano plot depicting the transcriptomic profiles of (A)
515 *Ldh* mutants ($Ldh^{16/17}$), (B) *Gpdh1* mutants ($Gpdh1^{A10/B18}$), and (C) double mutants
516 ($Gpdh1^{A10/B18}$; $Ldh^{16/17}$) relative to the respective heterozygous control strains. n=3
517 biological replicates analyzed per genotype. Each sample contained 20 mid-L2 larvae.
518 Vertical axis indicates -log10(FDR) and horizontal axis represents log(FC). The
519 significantly upregulated genes are shown in yellow and downregulated are shown in
520 black. FDR- fold discovery rate and FC-fold change.

521

522 **Supplementary Figure 6**. ***upd3; Gpdh1; Ldh* triple mutants exhibit a metabolomic**
523 **profile that is indistinguishable from *Gpdh1; Ldh* double mutants.** (A) A volcano plot
524 showing no significant difference between the metabolomes of *Gpdh1; Ldh* double
525 mutants and *upd3; Gpdh1; Ldh* triple mutants. (B-C) Relative abundance of (B) lactate
526 and (C) glycerol-3-phosphate in the indicated genotypes. n=6 biological replicates were
527 collected from independent populations with 25 mid L2 larvae per sample. Experiment
528 was repeated twice. Error bars represent standard deviation. No significant differences
529 (ns) were observed in in double mutants as compared with the triple mutants. *P*-value
530 was calculated by using the Mann-Whitney test. (D) Heatmap showing the top 25
531 metabolites rank order by significance among four genotypes - heterozygous control
532 (HC), $upd3^{\Delta}$ (U), $Gpdh1^{A10/B18}$; $Ldh^{16/17}$ double mutant (DM) and the *upd3Δ*; $Gpdh1^{A10/B18}$;
533 $Ldh^{16/17}$ triple mutants (TM).

534

535 **Supplementary Figure 7. *Stat-GFP* expression is increased in larval tissues of**
536 ***Gpdh1; Ldh* double mutants.** (A-L) Representative confocal images of (A-D) fat body,
537 (E-H) salivary glands and (I-L) muscles showing *Stat-GFP* expression in control,
538 $Gpdh1^{A10/B18}$, $Ldh^{16/17}$ and $Gpdh1^{A10/B18}$; $Ldh^{16/17}$ double mutants. The scale bar
539 represents 40 μM. The scale bar in (A) applies to (B-L).

540

541 **SUPPLEMENTARY TABLES**

542 **Table S1.** RNA-seq analysis of *Gpdh1*$^{A10/B18}$ single mutant larvae relative to *Gpdh1*$^{A10/+}$
543 heterozygous controls, *Ldh*$^{16/17}$ single mutant larvae relative to the *Ldh*$^{16/+}$ heterozygous
544 controls, and *Gpdh1*$^{A10/B18}$*; Ldh*$^{16/17}$ double mutant larvae relative to *Gpdh1*$^{A10/+}$*; Ldh*$^{16/+}$
545 heterozygous controls.

546

547 **Table S2.** A list of the genes that are significantly downregulated or upregulated in
548 *Gpdh1*$^{A10/B18}$*; Ldh*$^{16/17}$ double mutant larvae relative to *Gpdh1*$^{A10/+}$*; Ldh*$^{16/+}$ heterozygous
549 controls, but are expressed at normal levels in single mutant larvae.

550

551 **Table S3.** Metabolomic analysis of *Gpdh1*$^{A10/+}$*; Ldh*$^{16/+}$ heterozygous controls (HC), *upd3*$^{\Delta}$
552 single mutants (U), *Gpdh1*$^{A10/B18}$*; Ldh*$^{16/17}$ double mutant (DM), and *upd3*$^{\Delta}$*; Gpdh1*$^{A10/B18}$*;*
553 *Ldh*$^{16/17}$ triple mutants (TM).

554

555

556

557

558

559

REFERENCES

BAKER, S. A. & RUTTER, J. 2023. Metabolites as signalling molecules. *Nat Rev Mol Cell Biol,* 24**,** 355-374.

BAJGAR, A. & DOLEZAL, T. 2018. Extracellular adenosine modulates host-pathogen interactions through regulation of systemic metabolism during immune response in Drosophila. *PLoS Pathog,* 14**,** e1007022.

BAJGAR, A., KUCEROVA, K., JONATOVA, L., TOMCALA, A., SCHNEEDORFEROVA, I., OKROUHLIK, J. & DOLEZAL, T. 2015. Extracellular adenosine mediates a systemic metabolic switch during immune response. *PLoS Biol,* 13**,** e1002135.

BAWA, S., BROOKS, D. S., NEVILLE, K. E., TIPPING, M., SAGAR, M. A., KOLLHOFF, J. A., CHAWLA, G., GEISBRECHT, B. V., TENNESSEN, J. M., ELICEIRI, K. W. & GEISBRECHT, E. R. 2020. Drosophila TRIM32 cooperates with glycolytic enzymes to promote cell growth. *Elife,* 9.

BLAND, M. L. 2023. Regulating metabolism to shape immune function: Lessons from Drosophila. *Semin Cell Dev Biol,* 138**,** 128-141.

CARLSON, M. 2019. *Genome wide annotation for Fly.* [Online]. Available: https://bioconductor.org/packages/release/data/annotation/html/org.Dm.eg.db.html [Accessed].

CASTILLO-ARMENGOL, J., FAJAS, L. & LOPEZ-MEJIA, I. C. 2019. Inter-organ communication: a gatekeeper for metabolic health. *EMBO Rep,* 20**,** e47903.

DENG, H. & KERPPOLA, T. K. 2013. Regulation of Drosophila metamorphosis by xenobiotic response regulators. *PLoS Genet,* 9**,** e1003263.

DROUJININE, I. A. & PERRIMON, N. 2016. Interorgan Communication Pathways in Physiology: Focus on Drosophila. *Annual review of genetics,* 50**,** 539-570.

EKAS, L. A., BAEG, G. H., FLAHERTY, M. S., AYALA-CAMARGO, A. & BACH, E. A. 2006. JAK/STAT signaling promotes regional specification by negatively regulating wingless expression in Drosophila. *Development,* 133**,** 4721-9.

FIGLIA, G., WILLNOW, P. & TELEMAN, A. A. 2020. Metabolites Regulate Cell Signaling and Growth via Covalent Modification of Proteins. *Dev Cell,* 54**,** 156-170.

GERA, J., BUDAKOTI, P., SUHAG, M., MANDAL, L. & MANDAL, S. 2022. Physiological ROS controls Upd3-dependent modeling of ECM to support cardiac function in Drosophila. *Sci Adv,* 8**,** eabj4991.

GILLETTE, C. M., TENNESSEN, J. M. & REIS, T. 2021. Balancing energy expenditure and storage with growth and biosynthesis during Drosophila development. *Dev Biol,* 475**,** 234-244.

GRAMATES, L. S., AGAPITE, J., ATTRILL, H., CALVI, B. R., CROSBY, M. A., DOS SANTOS, G., GOODMAN, J. L., GOUTTE-GATTAT, D., JENKINS, V. K., KAUFMAN, T., LARKIN, A., MATTHEWS, B. B., MILLBURN, G., STRELETS, V. B. & THE FLYBASE, C. 2022. FlyBase: a guided tour of highlighted features. *Genetics,* 220.

GU, Z., EILS, R. & SCHLESNER, M. 2016. Complex heatmaps reveal patterns and correlations in multidimensional genomic data. *Bioinformatics,* 32**,** 2847-9.

JOHAN LARSSON, A. J. R. G., PETER GUSTAFSSON, DAVID H. EBERLY, EMANUEL HUBER, FLORIAN PRIVÉ. 2020. *eulerr: Area-Proportional Euler and Venn Diagrams with Ellipses* [Online]. Available: https://cran.r-project.org/web/packages/eulerr/index.html [Accessed].

KEVIN BLIGHE, A. L. 2020a. *PCAtools: everything Principal Component Analysis* [Online]. Github. Available: https://github.com/kevinblighe/PCAtools [Accessed].

KEVIN BLIGHE, S. R., MYLES LEWIS. 2020b. *EnhancedVolcano: publication-ready volcano plots with enhanced colouring and labeling* [Online]. Github. Available: https://github.com/kevinblighe/EnhancedVolcano [Accessed].

KIM, S. K., TSAO, D. D., SUH, G. S. B. & MIGUEL-ALIAGA, I. 2021. Discovering signaling mechanisms governing metabolism and metabolic diseases with Drosophila. *Cell Metab,* 33**,** 1279-1292.

KOYAMA, T., RODRIGUES, M. A., ATHANASIADIS, A., SHINGLETON, A. W. & MIRTH, C. K. 2014. Nutritional control of body size through FoxO-Ultraspiracle mediated ecdysone biosynthesis. *Elife,* 3.

KOYAMA, T., TEXADA, M. J., HALBERG, K. A. & REWITZ, K. 2020. Metabolism and growth adaptation to environmental conditions in Drosophila. *Cell Mol Life Sci,* 77**,** 4523-4551.

LI, H., RAI, M., BUDDIKA, K., STERRETT, M. C., LUHUR, A., MAHMOUDZADEH, N. H., JULICK, C. R., PLETCHER, R. C., CHAWLA, G., GOSNEY, C. J., BURTON, A. K., KARTY, J. A., MONTOOTH, K. L., SOKOL, N. S. & TENNESSEN, J. M. 2019. Lactate dehydrogenase and glycerol-3-phosphate dehydrogenase cooperatively regulate growth and carbohydrate metabolism during Drosophila melanogaster larval development. *Development,* 146.

LI, H. & TENNESSEN, J. M. 2017. Methods for studying the metabolic basis of Drosophila development. *Wiley Interdiscip Rev Dev Biol,* 6.

LI, H. & TENNESSEN, J. M. 2018. Preparation of Drosophila Larval Samples for Gas Chromatography-Mass Spectrometry (GC-MS)-based Metabolomics. *J Vis Exp*.

LIAO, T. S., CALL, G. B., GUPTAN, P., CESPEDES, A., MARSHALL, J., YACKLE, K., OWUSU-ANSAH, E., MANDAL, S., FANG, Q. A., GOODSTEIN, G. L., KIM, W. & BANERJEE, U. 2006. An efficient genetic screen in Drosophila to identify nuclear-encoded genes with mitochondrial function. *Genetics,* 174**,** 525-33.

LOVE, M. I., HUBER, W. & ANDERS, S. 2014. Moderated estimation of fold change and dispersion for RNA-seq data with DESeq2. *Genome Biol,* 15**,** 550.

MANDAL, S., GUPTAN, P., OWUSU-ANSAH, E. & BANERJEE, U. 2005. Mitochondrial regulation of cell cycle progression during development as revealed by the tenured mutation in Drosophila. *Dev Cell,* 9**,** 843-54.

MIYAZAWA, H. & AULEHLA, A. 2018. Revisiting the role of metabolism during development. *Development,* 145.

MUSSELMAN, L. P., FINK, J. L., GRANT, A. R., GATTO, J. A., TUTHILL, B. F., 2ND & BARANSKI, T. J. 2018. A Complex Relationship between Immunity and Metabolism in Drosophila Diet-Induced Insulin Resistance. Mol Cell Biol, 38.

NEMKOV, T., REISZ, J. A., GEHRKE, S., HANSEN, K. C. & D'ALESSANDRO, A. 2019. High-Throughput Metabolomics: Isocratic and Gradient Mass Spectrometry-Based Methods. Methods Mol Biol, 1978, 13-26.

ONO, H. 2014. Ecdysone differentially regulates metamorphic timing relative to 20-hydroxyecdysone by antagonizing juvenile hormone in Drosophila melanogaster. *Dev Biol,* 391**,** 32-42.

OZTURK-COLAK, A., MARYGOLD, S. J., ANTONAZZO, G., ATTRILL, H., GOUTTE-GATTAT, D., JENKINS, V. K., MATTHEWS, B. B., MILLBURN, G., DOS SANTOS, G., TABONE, C. J. & FLYBASE, C. 2024. FlyBase: updates to the Drosophila genes and genomes database. *Genetics,* 227.

PANG, Z., LU, Y., ZHOU, G., HUI, F., XU, L., VIAU, C., SPIGELMAN, A. F., MACDONALD, P. E., WISHART, D. S., LI, S. & XIA, J. 2024. MetaboAnalyst 6.0: towards a unified platform for metabolomics data processing, analysis and interpretation. *Nucleic Acids Res*.

PATRO, R., DUGGAL, G., LOVE, M. I., IRIZARRY, R. A. & KINGSFORD, C. 2017. Salmon provides fast and bias-aware quantification of transcript expression. *Nat Methods,* 14**,** 417-419.

PLETCHER, R. C., HARDMAN, S. L., INTAGLIATA, S. F., LAWSON, R. L., PAGE, A. & TENNESSEN, J. M. 2019. A Genetic Screen Using the Drosophila melanogaster TRiP RNAi Collection To Identify Metabolic Enzymes Required for Eye Development. *G3 (Bethesda),* 9**,** 2061-2070.

RAI, M., CARTER, S. M., SHEFALI, S. A., CHAWLA, G. & TENNESSEN, J. M. 2024. Characterization of genetic and molecular tools for studying the endogenous expression of Lactate dehydrogenase in Drosophila melanogaster. *PLoS One,* 19**,** e0287865.

RAJAN, A. & PERRIMON, N. 2011. Drosophila as a model for interorgan communication: lessons from studies on energy homeostasis. *Dev Cell,* 21**,** 29-31.

RECHSTEINER, M. C. 1970. Drosophila lactate dehydrogenase and alpha-glycerolphosphate

dehydrogenase: distribution and change in activity during development. *J Insect Physiol,* 16**,** 1179-92.

ROMAO, D., MUZZOPAPPA, M., BARRIO, L. & MILAN, M. 2021. The Upd3 cytokine couples inflammation to maturation defects in Drosophila. *Curr Biol,* 31**,** 1780-1787 e6.

SCHITO, L. & REY, S. 2018. Cell-Autonomous Metabolic Reprogramming in Hypoxia. *Trends Cell Biol,* 28**,** 128-142.

SONESON, C., LOVE, M. I. & ROBINSON, M. D. 2015. Differential analyses for RNA-seq: transcript-level estimates improve gene-level inferences. *F1000Res,* 4**,** 1521.

TENNESSEN, J. M., BAKER, K. D., LAM, G., EVANS, J. & THUMMEL, C. S. 2011. The Drosophila estrogen-related receptor directs a metabolic switch that supports developmental growth. *Cell Metab,* 13**,** 139-48.

TENNESSEN, J. M., BERTAGNOLLI, N. M., EVANS, J., SIEBER, M. H., COX, J. & THUMMEL, C. S. 2014. Coordinated metabolic transitions during Drosophila embryogenesis and the onset of aerobic glycolysis. *G3 (Bethesda),* 4**,** 839-50.

VANDER HEIDEN, M. G., CANTLEY, L. C. & THOMPSON, C. B. 2009. Understanding the Warburg effect: the metabolic requirements of cell proliferation. *Science,* 324**,** 1029-33.

WANG, Y. P. & LEI, Q. Y. 2018. Metabolite sensing and signaling in cell metabolism. *Signal Transduct Target Ther,* 3**,** 30.

WOODCOCK, K. J., KIERDORF, K., POUCHELON, C. A., VIVANCOS, V., DIONNE, M. S. & GEISSMANN, F. 2015. Macrophage-derived upd3 cytokine causes impaired glucose homeostasis and reduced lifespan in Drosophila fed a lipid-rich diet. *Immunity,* 42**,** 133-44.

YANG, H., KRONHAMN, J., EKSTROM, J. O., KORKUT, G. G. & HULTMARK, D. 2015. JAK/STAT signaling in Drosophila muscles controls the cellular immune response against parasitoid infection. *EMBO Rep,* 16**,** 1664-72.

YU, G. & HE, Q. Y. 2016. ReactomePA: an R/Bioconductor package for reactome pathway analysis and visualization. *Mol Biosyst,* 12**,** 477-9.

YU, G., WANG, L. G., HAN, Y. & HE, Q. Y. 2012. clusterProfiler: an R package for comparing biological themes among gene clusters. *OMICS,* 16**,** 284-7.

ZHU, A., IBRAHIM, J. G. & LOVE, M. I. 2019. Heavy-tailed prior distributions for sequence count data: removing the noise and preserving large differences. *Bioinformatics,* 35**,** 2084-2092.

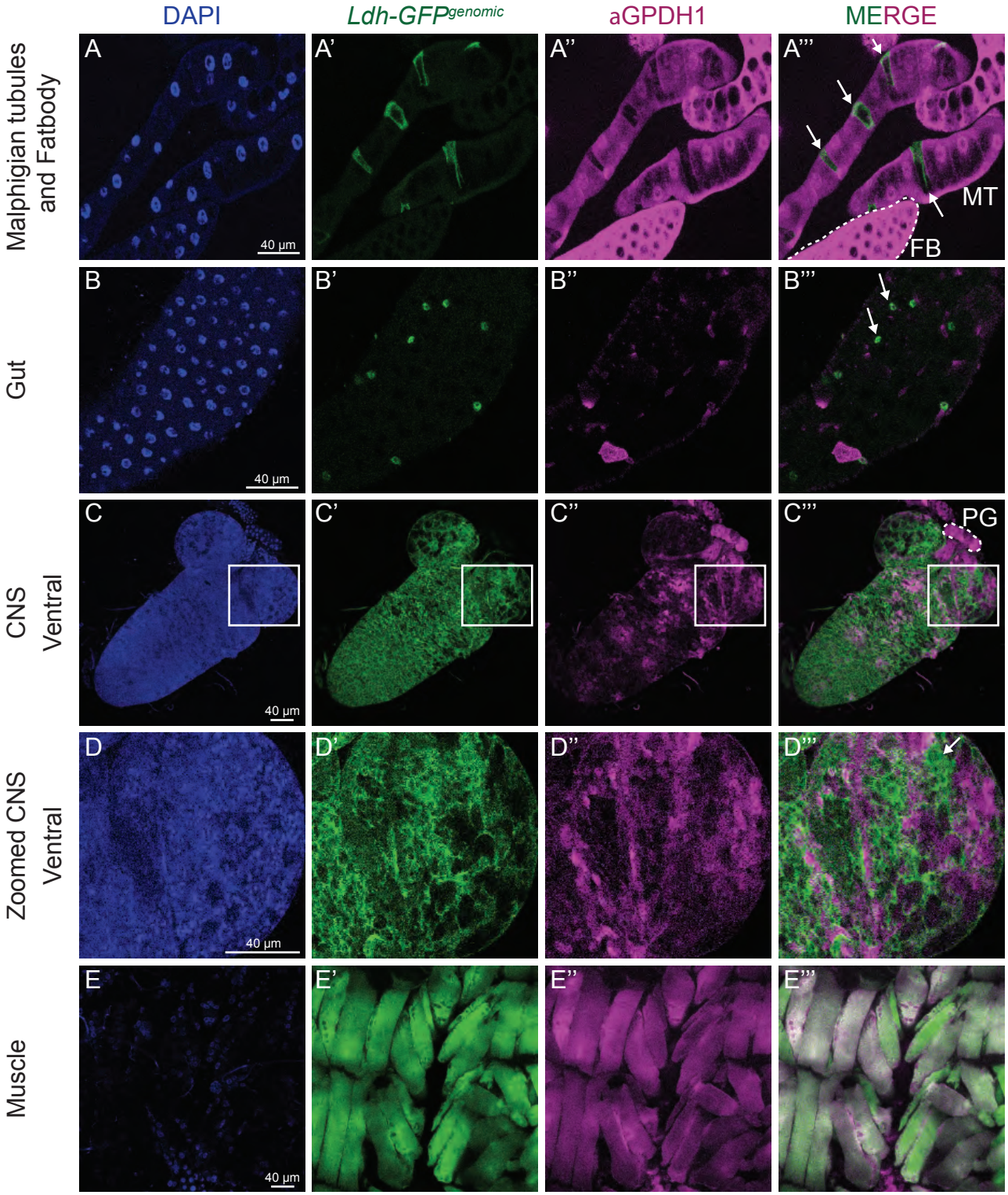
DAPI
Ldh-GFPgenomic
aGPDH1
MERGE
Malphigian tubules and Fatbody
Gut
CNS Ventral
Zoomed CNS Ventral
Muscle
A
A'
A''
A'''
MT
FB
B
B'
B''
B'''
C
C'
C''
C'''
PG
D
D'
D''
D'''
E
E'
E''
E'''
40 µm

Figure 1

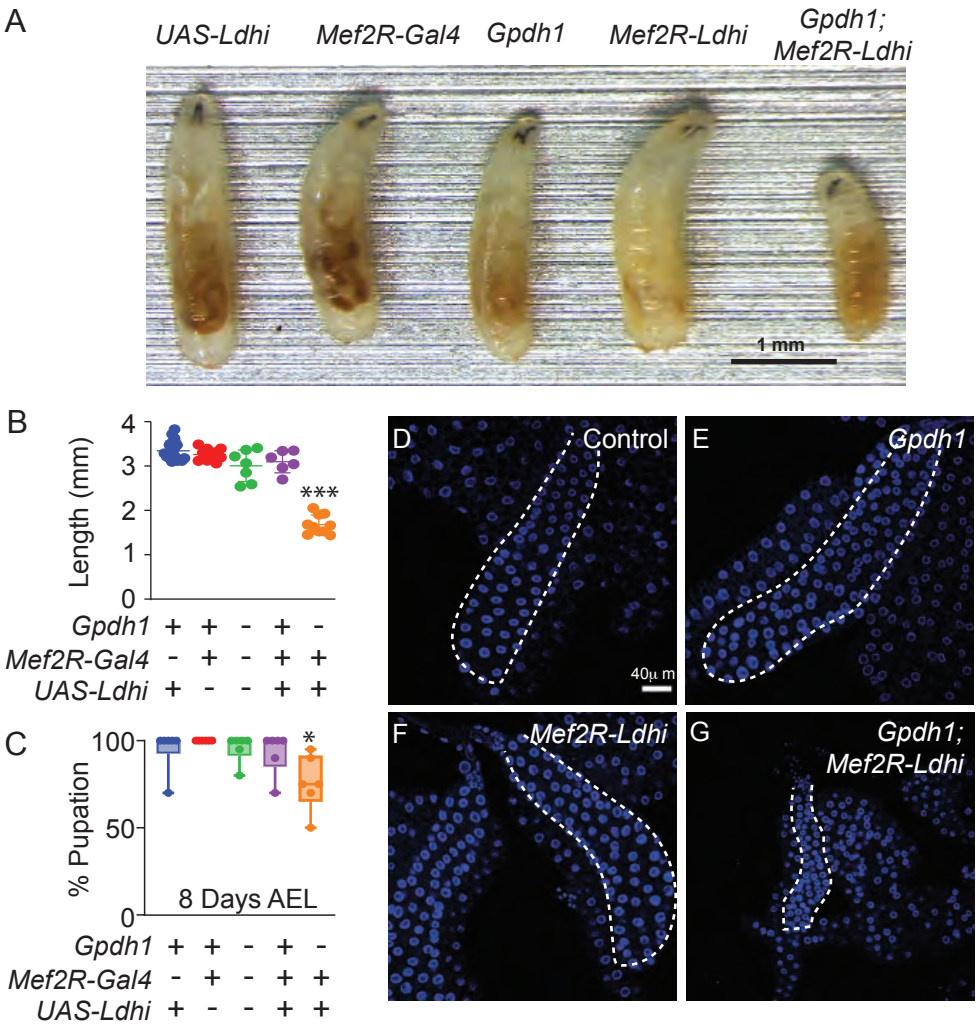
A
UAS-Ldhi
Mef2R-Gal4
Gpdh1
Mef2R-Ldhi
Gpdh1; Mef2R-Ldhi
1 mm
B
Length (mm)
4
3
2
1
0
***
Gpdh1 + + - + -
Mef2R-Gal4 - + - + +
UAS-Ldhi + - - + +
C
% Pupation
100
50
0
*
8 Days AEL
Gpdh1 + + - + -
Mef2R-Gal4 - + - + +
UAS-Ldhi + - - + +
D
Control
40μ m
E
Gpdh1
F
Mef2R-Ldhi
G
Gpdh1; Mef2R-Ldhi

Figure 2

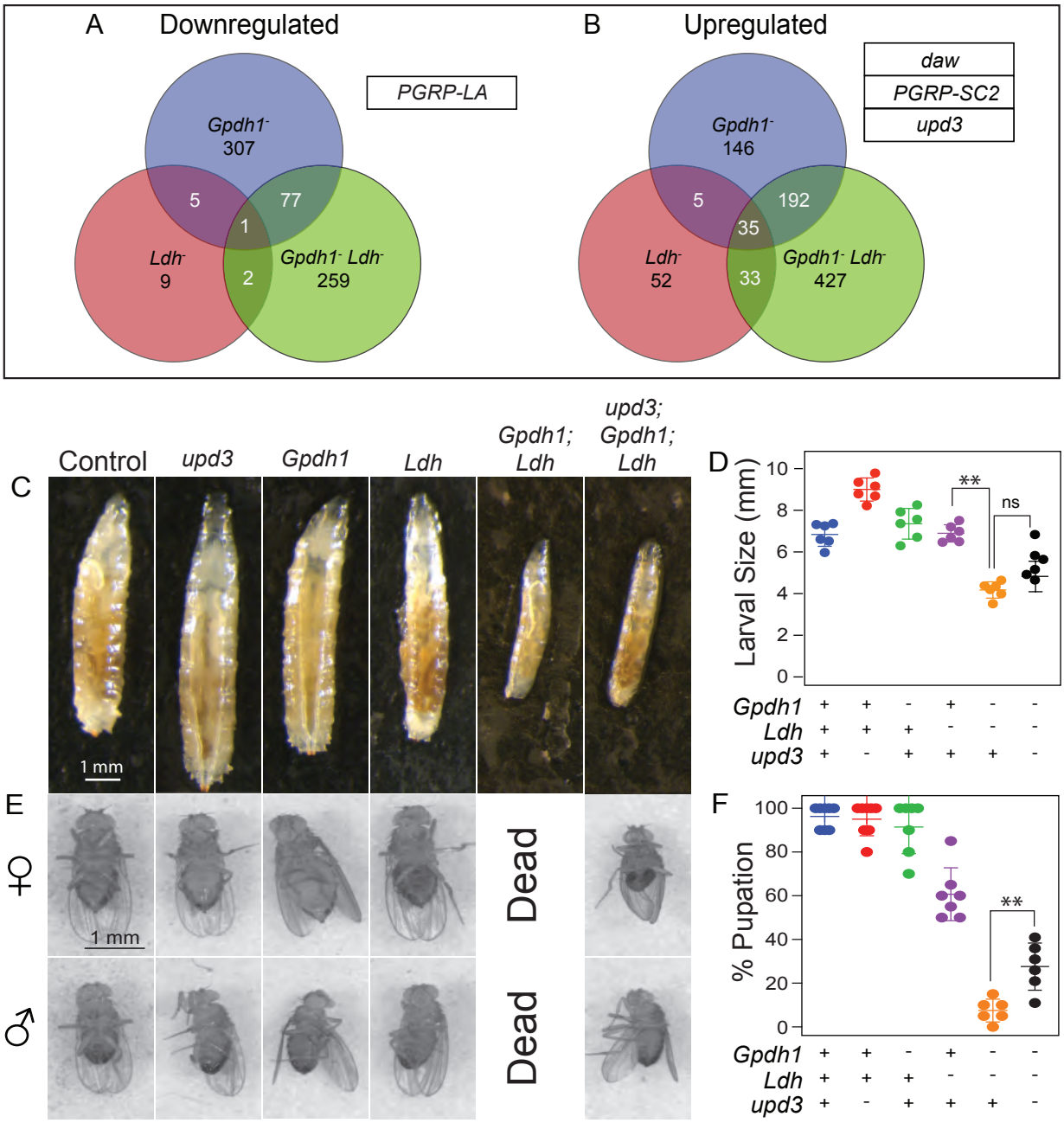
A
Downregulated
PGRP-LA
Gpdh1-
307
Ldh-
9
Gpdh1- Ldh-
259
5
77
1
2
B
Upregulated
daw
PGRP-SC2
upd3
Gpdh1-
146
Ldh-
52
Gpdh1- Ldh-
427
5
192
35
33
C
Control
upd3
Gpdh1
Ldh
Gpdh1; Ldh
upd3; Gpdh1; Ldh
1 mm
D
Larval Size (mm)
10
8
6
4
2
0
**
ns
Gpdh1 + + - + - -
Ldh + + + - - -
upd3 + - + + + -
E
♀
♂
1 mm
Dead
Dead
F
% Pupation
100
80
60
40
20
0
**
Gpdh1 + + - + - -
Ldh + + + - - -
upd3 + - + + + -

Figure 3

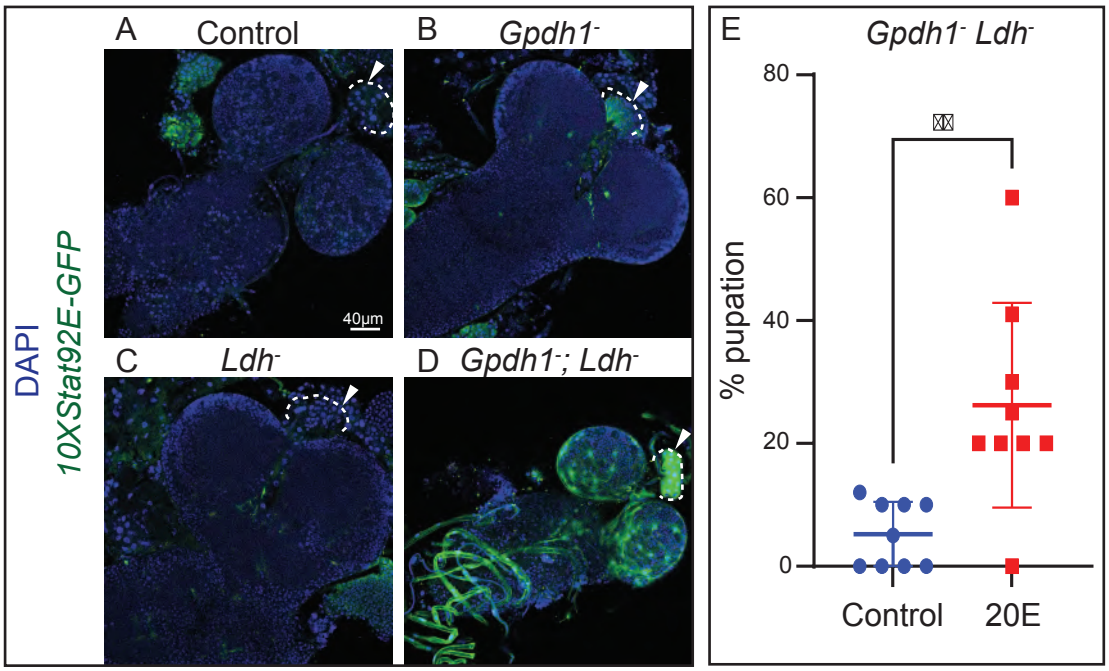
A
Control
B
Gpdh1-
C
Ldh-
D
Gpdh1-; Ldh-
DAPI
10XStat92E-GFP
40µm
E
Gpdh1- Ldh-
% pupation
80
60
40
20
0
Control
20E

Figure 4